# Near-Capacity Irregular Variable Length Coding and Irregular Unity Rate Coding

R. G. Maunder and L. Hanzo

*Abstract*—In this contribution we introduce an EXtrinsic Information Transfer (EXIT) chart matching technique for the design of two serially concatenated irregular codecs, each constituted by a variety of component codes. This approach facilitates a higher degree of design freedom than matching the EXIT function of an irregular codec to that of a regular codec, comprising only a single component code. As a result, a narrower EXIT chart tunnel can be created, facilitating operation at $E_b/N_0$ values that are closer to the channel's capacity bound. This is demonstrated for a serial concatenation of iteratively decoded Irregular Variable Length Coding (IrVLC) and Irregular Unity Rate Coding (IrURC), which is favourably compared with an IrVLC and regular Unity Rate Coding (URC) based benchmarker. Finally, we show that the iterative decoding complexity of our IrVLC-IrURC scheme can be reduced by about 25% upon employing a method of jointly performing EXIT chart matching, while seeking a reduced iterative decoding complexity.

*Index Terms*—Variable length codes, joint source and channel coding, trellis codes, information rates.

## I. INTRODUCTION

THE serial concatenation [1] and iterative decoding [2] of an irregular outer code with a regular inner code was proposed in [3]. Here, the irregular outer code comprises $N$ number of regular component codes $\{\mathbf{C}^n\}_{n=1}^N$ having a variety of inverted EXtrinsic Information Transfer (EXIT) functions $\{I_e^n(I_a)\}_{n=1}^N$ [4]. In the transmitter, each component encoder $\mathbf{C}^n$ is invoked to generate a specific fraction $\alpha^n$ of the encoded bit sequence. It was shown in [3] that the irregular decoder's composite EXIT function $I_e(I_a)$ may be obtained as a weighted average of the components' EXIT functions $\{I_e^n(I_a)\}_{n=1}^N$ according to $I_e(I_a) = \sum_{n=1}^N \alpha^n \cdot I_e^n(I_a)$. This property is exploited by the EXIT chart matching algorithm proposed in [3], which seeks the particular fractions $\{\alpha^n\}_{n=1}^N$ yielding an inverted EXIT function $I_e(I_a)$ that does not intersect the EXIT function of the serially concatenated inner decoder, in a manner similar to [5]. In this way, narrow but open EXIT chart tunnels can be created at near-capacity channel Signal to Noise Ratios (SNRs), facilitating iterative decoding convergence to an infinitesimally low probability of error [6].

However, we may expect to achieve even narrower open EXIT chart tunnels that facilitate operation even nearer to
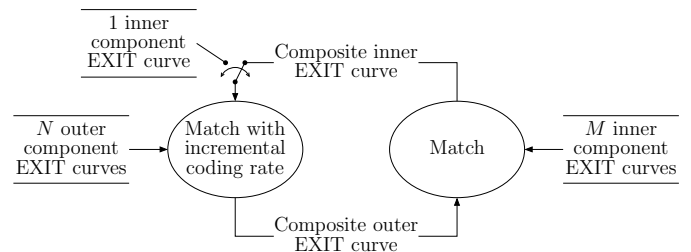
Fig. 1. Data-flow diagram of the iterative double EXIT chart matching algorithm.

capacity, if we could employ an irregular inner code as well as an irregular outer code, since this would provide a higher degree of design freedom. Hence, in Section II of this paper, we introduce a double EXIT chart matching algorithm, which allows the matching of the EXIT functions of two serially concatenated irregular codes to each other. Furthermore, in Section III we propose a modification to the EXIT chart matching algorithm of [3] that facilitates joint EXIT chart matching and the simultaneous quest for a reduced decoding complexity. We then design a transmission scheme that exemplifies the application of these algorithms in Section IV. We detail the choice of parameters for our proposed transmission scheme in Section V and analyse its performance in Section VI. Finally, we offer our conclusions in Section VII.

## II. DOUBLE EXIT CHART MATCHING

In this section we detail a double EXIT chart matching algorithm, which matches the composite EXIT functions of an outer and an inner irregular code, comprising $N$ and $M$ number of components, respectively. Here, the 'single' EXIT chart matching algorithm of [3] is iteratively applied in order to alternately match the outer EXIT function to the inner and vice versa, as illustrated in the data-flow diagram of Figure 1.

Note that the 'single' EXIT chart matching algorithm of [3] allows the design of an irregular code having a specific coding rate. This is exploited in the iterative double EXIT chart matching algorithm of Figure 1, which increments the coding rate of the irregular outer code in each iteration. Owing to the area property of EXIT charts [6], the open EXIT chart tunnel will therefore become narrower in each iteration, with the composite inner and outer EXIT functions converging to each other. In this way, an open EXIT tunnel may be maintained at near-capacity channel SNRs.

However, the iterative double EXIT chart matching algorithm of Figure 1 assumes that the inner irregular code is an

Irregular Unity Rate Code (IrURC). Similarly to its $M$ number of component Unity Rate Codes (URCs) [7], the IrURC has a unity coding rate, regardless of the particular irregular code design. Note that the 'single' EXIT chart matching algorithm may be adapted for this scenario by replacing $\mathbf{C}$ in Section VII and Table 1 of [3] with a vector $\mathbf{c} = \begin{bmatrix} 1 & 1 & \ldots & 1 \end{bmatrix}$ in which all $M$ number of elements are equal to unity and by replacing $\mathbf{d}$ with a unity-valued scalar $d = 1$. As a result, the matrix $\mathbf{T}$ of Section VII and Table 1 of [3] becomes a $M \times (M - 1)$ matrix, whose columns are a basis of the null space of $\mathbf{c}$ of dimension $M - 1$.

Note that at the commencement of the algorithm, no composite EXIT functions are available. For this reason, the algorithm begins with the matching of the composite outer EXIT function to a single one of the $M$ number of inner component's EXIT functions, as shown in Figure 1. The specific choice of the inner component EXIT function that fulfils this role is therefore a parameter of the iterative double EXIT chart matching algorithm. Following this, the iterative double EXIT matching algorithm continues, until the designed composite inner and outer EXIT functions intersect. At this point, the algorithm outputs the specific inner and outer component fractions found to maintain an open EXIT tunnel at the maximal coding rate.

Note that our attempts to devise a joint (as opposed to iterative) double EXIT chart matching algorithm were unsuccessful. Here, the matrix $\mathbf{A}$ in Section VII and Table 1 of [3] was adapted to include the EXIT functions of both the inner and outer irregular codes. However, we found that this modified algorithm did not reliably converge upon useful solutions.

## III. JOINT EXIT CHART MATCHING AND COMPLEXITY REDUCTION

As described in Section I, the algorithm of [3] may be adapted to additionally seek a reduced decoding complexity during EXIT chart matching. This is achieved by considering the decoding complexities associated with each of the $N$ number of component codes $\{\mathbf{C}^n\}_{n=1}^{N}$, when selecting the fractions $\{\alpha^n\}_{n=1}^{N}$. More specifically, the algorithm described in Section VII and Table 1 of [3] performs EXIT chart matching by employing the steepest descent approach to minimise a cost function $J(\alpha) = ||\mathbf{e}||_2^2 = \mathbf{e}^T\mathbf{e}$, where $\mathbf{e}$ is a vector of distances between the irregular outer code's inverted EXIT function and the serially concatenated inner code's EXIT function. We employ a vector $\mathbf{o}$ having a length $N$, specifying the *A Posteriori* Probability (APP) Soft-In Soft-Out (SISO) decoding complexity of each component code $\mathbf{C}^n$. Here, the decoding complexity is quantified by the average number $O(\mathbf{C}^n)$ of Add, Compare and Select (ACS) operations performed per Logarithmic Likelihood Ratio (LLR) [8] by the Bahl-Cocke-Jelinek-Raviv (BCJR) algorithm [9] operating in the logarithmic probability domain and using an eight-entry lookup table for correcting the Jacobian approximation [10]. In a manner similar to (15) of [11], the cost function of [3] may be adapted to consider the irregular APP SISO decoder's computational complexity according to

$$J(\alpha) = ||\mathbf{e}||_2^2 + y^2||\mathbf{o}^T\alpha||_2^2, \tag{1}$$

where $y$ is a scalar value, which assumes a positive value that is commensurate with the relative importance of seeking a low computational complexity for the APP SISO decoder, or a zero value if this complexity should not be considered during EXIT chart matching.

During the steepest descent approach of [3], the gradient $\mathbf{e_b}$ of the cost function $J(\alpha)$ is evaluated with respect to a vector $\beta$ that is dependent on the vector $\alpha$ listing the constituent codes' fractions. This gradient $\mathbf{e_b}$ is employed to iteratively update the vector $\beta$, and hence the fractions vector $\alpha$, in order to converge towards a minimal cost function $J(\alpha)$. The EXIT chart matching algorithm may be adapted to additionally seek a reduced APP SISO decoding computational complexity by employing the cost function of (1) during the derivation of $\mathbf{e}_b$ and $\beta$. With reference to Section VII and Table 1 of [3], the revised $\mathbf{e}_b$ and $\beta$ are specified by

$$\begin{aligned}\mathbf{e}_b = \ & (\mathbf{T}^T\mathbf{A}^T\mathbf{A}\mathbf{T} + y^2\mathbf{T}^T\mathbf{o}\mathbf{o}^T\mathbf{T})\beta - \\ & \mathbf{T}^T\mathbf{A}^T(\mathbf{b} - \mathbf{A}\alpha_c) + y^2\mathbf{T}^T\mathbf{o}\mathbf{o}^T\alpha_c\end{aligned}$$

and

$$\beta = \beta - \mathbf{e}_b^T\mathbf{e}_b/(\mathbf{e}_b^T(\mathbf{T}^T\mathbf{A}^T\mathbf{A}\mathbf{T} + y^2\mathbf{T}^T\mathbf{o}\mathbf{o}^T\mathbf{T})\mathbf{e}_b)\cdot\mathbf{e}_b,$$

respectively.

## IV. OVERVIEW OF THE TRANSMISSION SCHEME CONSIDERED

In this section we consider a transmission scheme that facilitates the iterative joint source and channel decoding [12]–[17] of a sequence of source symbols having values with unequal probabilities of occurrence for near-capacity transmission over an uncorrelated narrowband Rayleigh fading channel. We employ $K = 16$-ary source symbol values obeying the probabilities of occurrence that result from the Lloyd-Max quantization [18] [19] of independent Gaussian distributed source samples, giving a source entropy of $E = 3.77$ bits/symbol. This application motivates the employment of Irregular Variable Length Coding (IrVLC), as discussed in [20]. This outer codec is serially concatenated and iteratively decoded with an IrURC used as the inner codec, as shown in the schematic of Figure 2. Since this combined IrVLC-IrURC scheme employs two irregular codecs, it allows us to exemplify double EXIT chart matching, as proposed in this paper.

In the IrVLC-IrURC scheme of Figure 2, the outer IrVLC arrangement employs $N$ number of component VLEC codebooks $\{\mathbf{VLEC}^n\}_{n=1}^{N}$ having different EXIT functions for generating particular fractions of the encoded bit sequence [20]. Similarly, the inner IrURC arrangement employs $M$ number of component URC codes $\{\mathbf{URC}^m\}_{m=1}^{M}$ [7].

In the transmitter shown in Figure 2, the source symbol frame $\mathbf{s}$ and the IrVLC-encoded bit frame $\mathbf{u}$ are comprised of $N$ number of components, which are encoded by the corresponding component VLEC codes $\{\mathbf{VLEC}^n\}_{n=1}^{N}$. Each source symbol frame component $\mathbf{s}^n$ comprises $J^n$ number of source symbols, where $\sum_{n=1}^{N} J^n = J$. Note that the fractions $J^n/J$ of the source symbol frame $\mathbf{s}$ that are encoded by each component VLEC code $\mathbf{VLEC}^n$ may be chosen in order to shape the inverted IrVLC EXIT function, as will
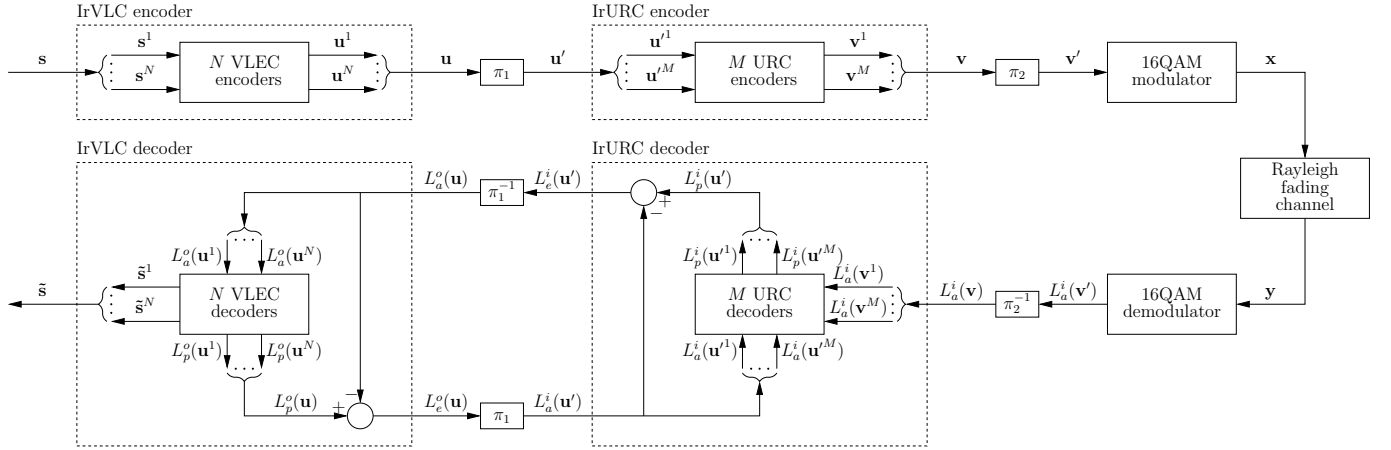
Fig. 2.    Schematic of the IrVLC-IrURC scheme.

be detailed in Section V. Similarly, each IrVLC-encoded bit frame component $\mathbf{u}^n$ comprises a number $I^n$ of bits that will typically vary from frame to frame owing to the variable lengths of the VLEC codewords, where $\sum_{n=1}^{N} I^n = I$.

In order to facilitate the VLEC decoding of the IrVLC-encoded bit frame components $\{\mathbf{u}^n\}_{n=1}^{N}$, it is necessary to explicitly convey their lengths $\{I^n\}_{n=1}^{N}$ to the receiver. Furthermore, this highly error sensitive side information must be reliably protected against transmission errors, using a powerful low rate block code, for example. For the sake of avoiding obfuscation, this is not shown in Figure 2. Note that since the amount of the encoded side information is typically negligible compared to the length of the IrVLC-encoded bit frame components $\{\mathbf{u}^n\}_{n=1}^{N}$ [20], we do not consider it any further in this paper.

The interleaved IrVLC-encoded bit frame $\mathbf{u}'$ provided by the $I$-bit random interleaver $\pi_1$ and the IrURC-encoded bit frame $\mathbf{v}$ are comprised of $M$ number of components, which are encoded by the corresponding component URC codes $\{\mathbf{URC}^m\}_{m=1}^{M}$. Each interleaved IrVLC-encoded bit frame component $\mathbf{u}'^m$, as well as the corresponding IrURC-encoded bit frame component $\mathbf{v}^m$, comprises $I^m$ number of bits, where $\sum_{m=1}^{M} I^m = I$. Note that the fractions $I^m/I$ of the interleaved IrVLC-encoded bit frame $\mathbf{u}'$ that are encoded by each component URC code $\mathbf{URC}^m$ may be chosen in order to shape the IrURC EXIT function, as will be detailed in Section V.

Finally, the interleaved IrURC-encoded bit frame $\mathbf{v}'$ provided by the $I$-bit random interleaver $\pi_2$ is modulated onto the Rayleigh fading channel using Gray-mapped 16-ary Quadrature Amplitude Modulation (16QAM) [21].

In the receiver, APP SISO IrURC- and IrVLC-decoding are performed iteratively, as shown in Figure 2. Both of these decoders invoke the BCJR algorithm [9] applied to the bit-based trellises [22], [23]. The extrinsic soft information, represented in the form of LLRs [8], is iteratively exchanged between the IrURC and IrVLC decoding stages for the sake of assisting each other's operation as usual [2]. In Figure 2, $L(\cdot)$ denotes the LLRs of the bits concerned, where the superscript $i$ indicates inner IrURC decoding, while $o$ corresponds to outer IrVLC decoding. Additionally, a subscript denotes the

TABLE I
CONSIDERED PARAMETERISATIONS OF THE IrVLC-IrURC SCHEME.

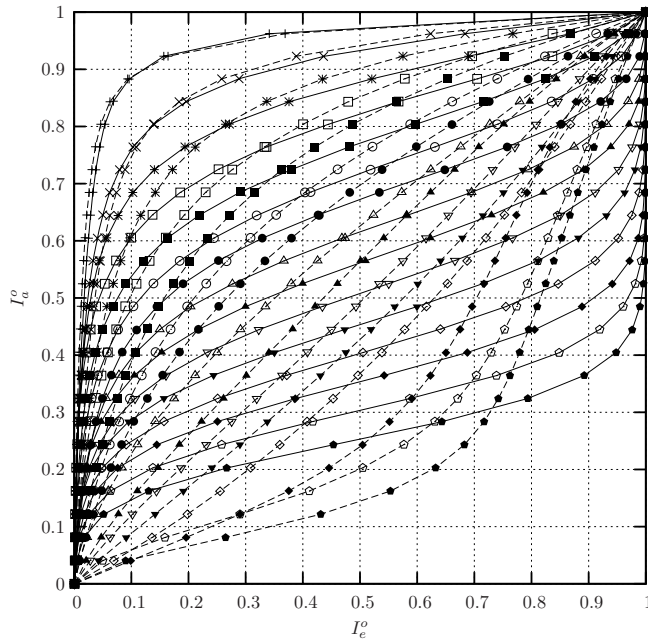| Parameterisation | $N$ | $M$ | IrVLC $y$ | IrURC $y$ |
|---|---|---|---|---|
| IrVLC-IrURC-high | 30 | 10 | 0 | 0 |
| IrVLC-IrURC-low | 30 | 10 | $10^{-5}$ | 0 |
| IrVLC-URC-high | 30 | 1 | 0 | N/A |
| IrVLC-URC-low | 30 | 1 | $10^{-5}$ | N/A |

dedicated role of the LLRs, with $a$, $p$ and $e$ indicating *a priori*, *a posteriori* and extrinsic information, respectively. Following the final decoding iteration, bit-based MAP VLEC sequence estimation is performed as usual [20], yielding the reconstructed source symbol frame estimate $\tilde{\mathbf{s}}$, as shown in Figure 2.

## V. SYSTEM PARAMETER DESIGN

In this section we introduce four different parameterisations of the IrVLC-IrURC scheme of Section IV. We refer to these as the IrVLC-IrURC-high, the IrVLC-IrURC-low, the IrVLC-URC-high and the IrVLC-URC-low parameterisations, which are summarized in Table I.

In each of the four IrVLC-IrURC parameterisations considered, we elected to employ an IrVLC comprising $N = 30$ component VLEC codebooks $\{\mathbf{VLEC}^n\}_{n=1}^{30}$, which is sufficient to represent the variety of the possible inverted VLEC EXIT function shapes. More specifically, the $N = 30$ component VLEC codebooks $\{\mathbf{VLEC}^n\}_{n=1}^{30}$ were designed using the genetic algorithm of [24] to have a wide range of coding rates $\{R(\mathbf{VLEC}^n)\}_{n=1}^{30}$ and Real-Valued Free Distance Metrics (RV-FDMs) $\{D(\mathbf{VLEC}^n)\}_{n=1}^{30}$. Maximal RV-FDMs were sought for coding rates in the range of $[0.25, 0.95]$ during the generation of the first 15 of the $N = 30$ component VLEC codebooks $\{\mathbf{VLEC}^n\}_{n=1}^{15}$ [24]. By contrast, RV-FDMs as close to, but no less than 2 were sought during the generation of the remaining 15 VLEC codebooks $\{\mathbf{VLEC}^n\}_{n=16}^{30}$, which have coding rates in the range of $[0.25, 0.95]$. For reasons of space economy, the composition of the $N = 30$ component VLEC codebooks is not provided in this paper.

The inverted EXIT functions of the $N = 30$ component VLEC codebooks $\{\mathbf{VLEC}^n\}_{n=1}^{30}$ are provided in Figure 3.

Fig. 4. EXIT functions for the $M = 10$ component URC codes $\{\mathbf{URC}^m\}_{m=1}^{10}$ for a 16QAM-modulated Rayleigh fading channel SNR of $E_c/N_0 = 8$ dB. Functions are labelled using the format $\mathbf{URC}$ $(g(\mathbf{URC}), f(\mathbf{URC}))$, where $g(\mathbf{URC})$ and $f(\mathbf{URC})$ are the hexadecimal generator and feedback polynomials of the URC code, respectively [10].

VLEC$^1$ (0.950, 2.412, 1781) —+— VLEC$^{16}$(0.952, 2.394, 1820) --+--
VLEC$^2$ (0.900, 2.518, 1950) —×— VLEC$^{17}$(0.901, 2.373, 1906) --×--
VLEC$^3$ (0.850, 2.617, 2232) —∗— VLEC$^{18}$(0.851, 2.357, 1952) --∗--
VLEC$^4$ (0.800, 2.710, 2587) —▫— VLEC$^{19}$(0.800, 2.312, 2333) --▫--
VLEC$^5$ (0.750, 2.793, 2761) —■— VLEC$^{20}$(0.750, 2.308, 2290) --■--
VLEC$^6$ (0.701, 2.922, 2994) —○— VLEC$^{21}$(0.700, 2.275, 2662) --○--
VLEC$^7$ (0.650, 2.981, 3577) —●— VLEC$^{22}$(0.653, 2.269, 2980) --●--
VLEC$^8$ (0.601, 4.364, 4489) —△— VLEC$^{23}$(0.605, 2.257, 2991) --△--
VLEC$^9$ (0.550, 4.628, 5694) —▲— VLEC$^{24}$(0.553, 2.225, 2966) --▲--
VLEC$^{10}$ (0.501, 4.807, 6934) —▽— VLEC$^{25}$(0.501, 2.133, 3327) --▽--
VLEC$^{11}$ (0.450, 5.869, 8424) —▼— VLEC$^{26}$(0.451, 2.133, 3808) --▼--
VLEC$^{12}$ (0.400, 6.573, 10677) —◇— VLEC$^{27}$(0.407, 2.113, 4445) --◇--
VLEC$^{13}$ (0.350, 8.475, 13463) —◆— VLEC$^{28}$(0.350, 2.155, 6719) --◆--
VLEC$^{14}$ (0.301, 10.384, 19658) —○— VLEC$^{29}$(0.300, 2.123, 8112) --○--
VLEC$^{15}$ (0.251, 12.449, 25265) —●— VLEC$^{30}$(0.252, 2.117, 11824) --●--

Fig. 3. Inverted EXIT functions for the $N = 30$ component VLEC codebooks $\{\mathbf{VLEC}^n\}_{n=1}^{30}$. Functions are labelled using the format $\mathbf{VLEC}$ $(R(\mathbf{VLEC}), D(\mathbf{VLEC}), O(\mathbf{VLEC}))$.

For each considered VLEC codebook $\mathbf{VLEC}$, the coding rate $R(\mathbf{VLEC})$ and RV-FDM $D(\mathbf{VLEC})$ are provided in Figure 3. Furthermore, the computational complexity of APP SISO decoding is characterised by the average number $O(\mathbf{VLEC})$ of ACS operations performed per source symbol per decoding iteration.

Note that 'S'-shaped inverted EXIT functions having up to two points of inflection are obtained in Figure 3 for the VLEC codebooks $\{\mathbf{VLEC}^n\}_{n=1}^{15}$, which have high RV-FDMs [24]. By contrast, the low RV-FDM VLEC codebooks $\{\mathbf{VLEC}^n\}_{n=16}^{30}$ are associated with EXIT functions having no more than a single point of inflection. Since the suite of $N = 30$ VLEC codebooks $\{\mathbf{VLEC}^n\}_{n=1}^{30}$ is associated with a wide variety of inverted EXIT functions, it is particularly suitable for use in IrVLCs [24]. Also note that the high RV-FDM VLEC codebooks $\{\mathbf{VLEC}^n\}_{n=1}^{15}$ are associated with higher APP SISO decoder complexities than the low RV-FDM VLEC codebooks $\{\mathbf{VLEC}^n\}_{n=16}^{30}$.

In the same way that the IrVLC-IrURC scheme employs $N$ number of component VLEC codebooks, it also employs $M$ number of component URC codes, as described in Section IV. However, the value of $M$ varies amongst our parameterisations considered. In the case of the IrVLC-IrURC-high and the IrVLC-IrURC-low parameterisations of Table I, we elected
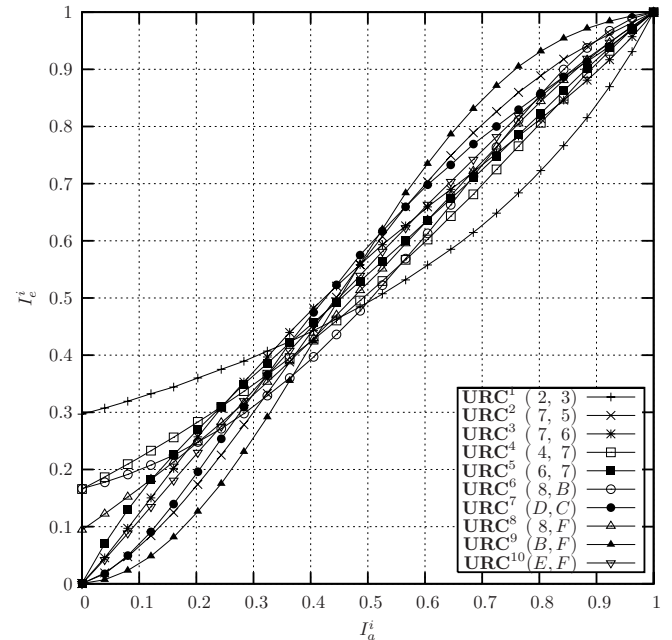
to employ $M = 10$ component URC codes $\{\mathbf{URC}^m\}_{m=1}^{10}$, which is sufficient to represent the variety of the possible URC EXIT function shapes. More specifically, our $M = 10$ component URC codes $\{\mathbf{URC}^m\}_{m=1}^{10}$ were selected from the set of all possible URC code designs that have shift register representations containing no more than three memory elements in order to yield a variety of EXIT function shapes, as provided in Figure 4. The generator and feedback polynomials of the component URC codes $\{\mathbf{URC}^m\}_{m=1}^{10}$ are provided in Figure 4. Note that some URC component EXIT functions emerge from the $(0,0)$ point of the EXIT chart, whilst others offer some non-zero extrinsic information even in the absence of any *a priori* information.

By contrast, the benchmarker IrVLC-URC-high and IrVLC-URC-low parameterisations employ just $M = 1$ component URC code and can therefore be deemed to employ regular URCs instead of IrURCs. Since these benchmarkers employ only one irregular code, they must employ the 'single' EXIT chart matching algorithm of [3] and hence, in contrast to the IrVLC-IrURC-high and IrVLC-IrURC-low parameterisations, they cannot benefit from the more general double EXIT chart matching method of Section II. As a result, we may expect the IrVLC-IrURC-high and IrVLC-IrURC-low parameterisations to outperform their corresponding benchmarkers of IrVLC-URC-high and IrVLC-URC-low, respectively. In order to demonstrate this, the URC code offering the best potential EXIT chart match was selected from the set $\{\mathbf{URC}^m\}_{m=1}^{10}$ for use in the IrVLC-URC-high and IrVLC-URC-low benchmarkers. This was identified as $\mathbf{URC}^8$, since its EXIT function emerges from the lowest non-zero point along the $I_e^i$ axis at $I_a^i = 0$ in the EXIT chart provided in Figure 4.

Note that in the case of the IrVLC-IrURC-low and IrVLC-URC-low parameterisations, the method of Section III was used for jointly performing EXIT chart matching and for reducing the corresponding APP SISO decoder's computational complexity. In both cases, a weighting coefficient of $y = 10^{-5}$ was employed when designing the IrVLC scheme, as shown in Table I, while $y = 0$ was used for the IrURC scheme of the IrVLC-IrURC-low parameterisation. For this parameterisation, we elected to reduce the computational complexity of only the IrVLC scheme, but not of the IrURC scheme, since the computational complexity of IrVLCs is typically significantly higher than that of IrURCs.

For each parameterisation, EXIT chart matching was performed for a number of 16QAM-modulated Rayleigh fading channel SNRs in the range of $E_c/N_0 \in [3.5, 20.5]$ dB. Since the IrURC and URC arrangements have unity coding rates and because 16QAM modulation is employed in all parameterisations, the effective throughput of each parameterisation is given by $\eta = R \cdot \log_2(16)$ bits per channel use, where $R$ is the IrVLC coding rate. Additionally, note that the channel SNR values of $E_c/N_0$ may be converted to $E_b/N_0$ values according to $E_b/N_0 = E_c/N_0 \cdot 1/\eta$, where $N_0$ is the noise power spectral density and $E_c$ as well as $E_b$ are the transmit energy per channel use and per bit of source information, respectively. Figure 5 plots the maximum effective throughput $\eta$ for which open EXIT chart tunnels could be created for each parameterisation over a range of 16QAM modulated Rayleigh fading channel $E_b/N_0$ values. Note that Figure 5 also provides a plot of the Discrete-input Continuous-output Memoryless Channel (DCMC) capacity [25] versus $E_b/N_0$ [21]. In addition to this, Figure 5 provides a plot of the *attainable* capacity, which is reduced owing to the capacity loss associated with employing 'one-shot' demodulation instead of including the demodulator in the iterative decoding process shown in Figure 2. The attainable capacity for a particular $E_b/N_0$ value was estimated [6] upon multiplying the average area beneath the corresponding EXIT functions of the $M = 10$ component URC codes by $\log_2(16) = 4$, since 16QAM modulation is employed.

In Figure 5, the IrVLC-IrURC-high and IrVLC-IrURC-low parameterisations can be seen to consistently achieve open EXIT chart tunnels at higher effective throughputs than the corresponding IrVLC-URC-high and IrVLC-URC-low parameterisations. This may be explained by the higher degree of design freedom that is facilitated by double EXIT chart matching.

Observe in Figure 5 that the IrVLC-IrURC-high and IrVLC-IrURC-low parameterisations offer the highest gain over the corresponding IrVLC-URC-high and IrVLC-URC-low parameterisations at an effective throughput of $\eta = 2.12$ bits per channel use. In order that we may assess the potential benefits of double EXIT chart matching, the remainder of this paper therefore considers arrangements of the four parameterisations that have an effective throughput of $\eta = 2.12$ bits per channel use. The threshold $E_b/N_0$ values for which these arrangements can achieve open EXIT chart tunnels are indicated in Figure 5, together with the corresponding DCMC capacity bound and attainable capacity bound. Furthermore, the marginally open EXIT chart tunnels of the IrVLC-IrURC-high, IrVLC-IrURC-
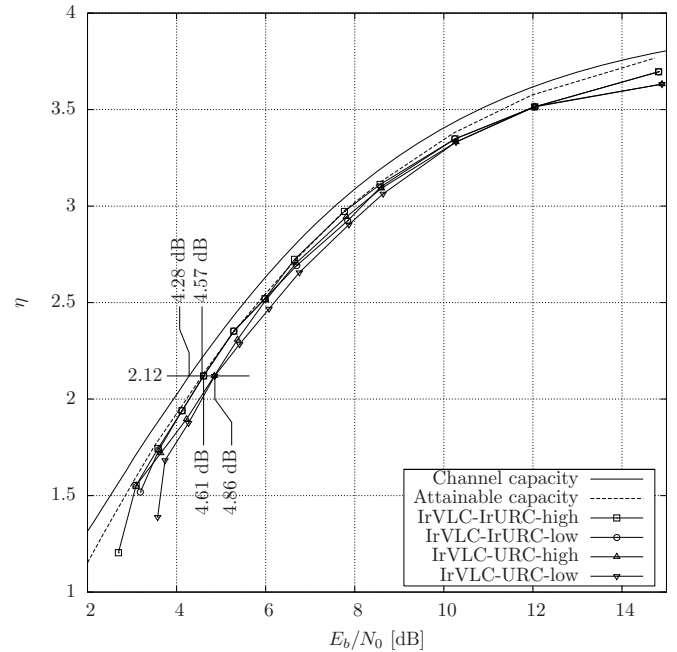


Fig. 5. The maximum effective throughput for which open EXIT chart tunnels could be achieved versus 16QAM-modulated Rayleigh fading channel $E_b/N_0$ for the IrVLC-IrURC-high, IrVLC-IrURC-low, IrVLC-URC-high and IrVLC-URC-low parameterisations of Table I. Plots of the DCMC capacity and attainable capacity are additionally provided [21].
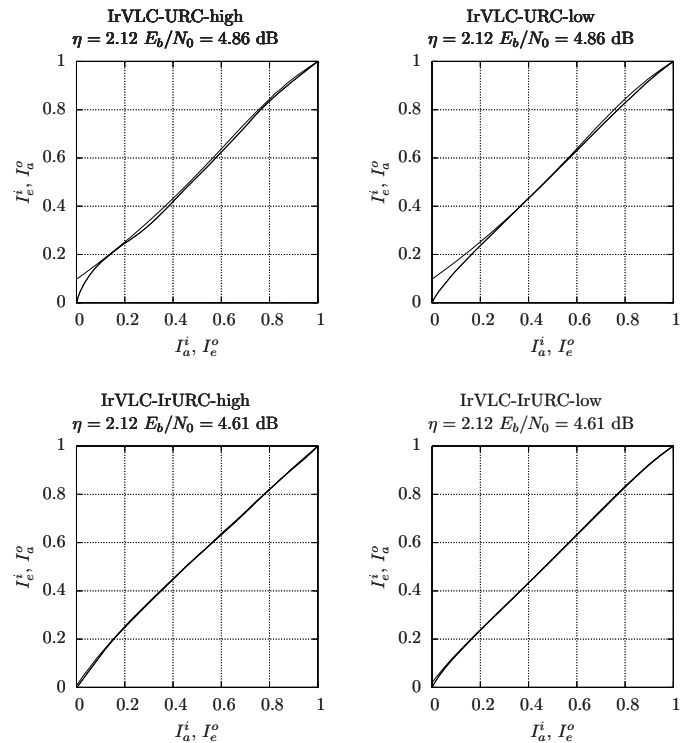


Fig. 6. Marginally open EXIT chart tunnels of the IrVLC-IrURC-high, IrVLC-IrURC-low, IrVLC-URC-high and IrVLC-URC-low arrangements.

low, IrVLC-URC-high and IrVLC-URC-low arrangements are provided in Figure 6.

Note that owing to the area property of EXIT charts [6], the narrow EXIT chart tunnels shown in Figure 6 for the IrVLC-IrURC-high and IrVLC-IrURC-low arrangements yield

TABLE II
MINIMUM $E_b/N_0$ VALUES AT WHICH AN SER OF $10^{-3}$ MAY BE ACHIEVED.

| Parameterisation | Minimum $E_b/N_0$ value | | | |
|---|---|---|---|---|
| | $I \approx 10^6$ | $I \approx 10^5$ | $I \approx 10^4$ | $I \approx 10^3$ |
| IrVLC-IrURC-high | 4.71 dB | 5.06 dB | 7.85 dB | 14.27 dB |
| IrVLC-IrURC-low | 4.71 dB | 5.38 dB | 7.59 dB | 11.32 dB |
| IrVLC-URC-high | 4.97 dB | 5.11 dB | 6.23 dB | 8.87 dB |
| IrVLC-URC-low | 4.87 dB | 5.66 dB | 8.17 dB | 12.63 dB |

the threshold $E_b/N_0$ value of Figure 5 that is only 0.04 dB from the attainable capacity bound. Here, the presence of the component URC codes having the EXIT functions of Figure 4 that emerge from the $(0,0)$ point facilitates the design of an IrURC EXIT function that starts close to the point where the inverted IrVLC EXIT function begins. By contrast, much of the marginally open EXIT chart tunnel area shown in Figure 6 for the IrVLC-URC-high and IrVLC-URC-low arrangements is a consequence of having a relatively high starting point of $(0, 0.1)$ in the URC's EXIT function.

## VI. RESULTS

In this section, the achievable performance of the IrVLC-IrURC-high, the IrVLC-IrURC-low, the IrVLC-URC-high and the IrVLC-URC-low arrangements of Section V is characterised and our quantitative findings are presented. In each case, we simulated the transmission of $1\,406\,400$ source symbols, which were arranged in frames **s** in order to yield four different average interleaver lengths of $I = JE/R \approx \{10^6, 10^5, 10^4, 10^3\}$ bits. These interleaver lengths are practical in wireless multimedia broadcast applications for example, where coded bit rates of about 40 Mbit/s are typical [26].

During the decoding of each frame, the iterative decoding process was continued until it offered no further improvements for the source symbol frame estimate $\tilde{\mathbf{s}}$, whereupon the corresponding non-Levenshtein Symbol Error Ratio (SER) was recorded. The minimum $E_b/N_0$ values required to achieve an SER below $10^{-3}$ for each interleaver length considered are provided in Table II.

Observe in Table II that, when employing the long average interleaver lengths of $I \approx 10^6$ and $I \approx 10^5$, the IrVLC-IrURC-high and IrVLC-IrURC-low arrangements facilitate operation at lower $E_b/N_0$ values than the corresponding IrVLC-URC-high or IrVLC-URC-low arrangement, as predicted in Section V. Indeed, for $I \approx 10^6$, the discrepancies between the attainable channel capacity of 4.57 dB and the $E_b/N_0$ values recorded for the IrVLC-IrURC-high and IrVLC-IrURC-low arrangements are less than half of those for the IrVLC-URC-high and IrVLC-URC-low arrangements. We therefore consider this gain to be significant.

However, when short interleavers are invoked, the IrVLC-IrURC-high arrangement is shown to be outperformed by the IrVLC-URC-high arrangement in Table II. This may be explained by considering the IrVLC-URC-high arrangement's marginally open EXIT chart tunnel, which is narrow at only one point along its length, as shown in Figure 6. As a result, the IrVLC-URC-high arrangement has a lower sensitivity to correlation within the *a priori* LLR frames than the other
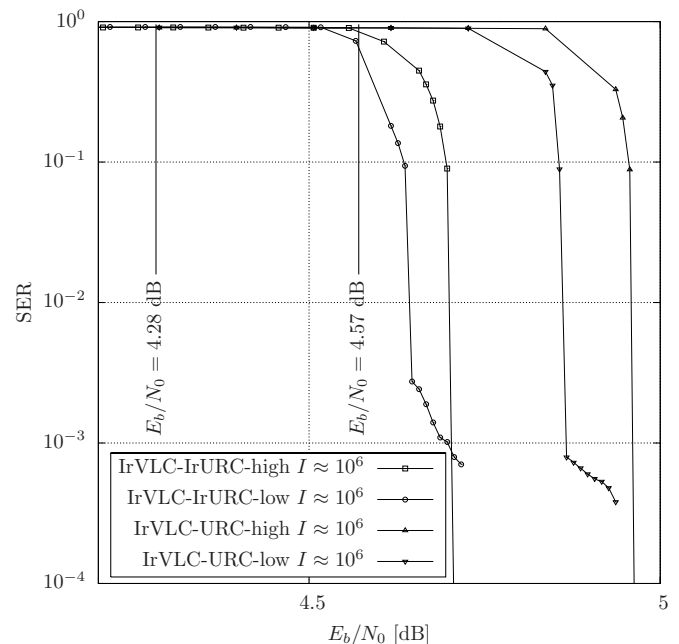


Fig. 7. The SERs achieved by the various arrangements of the IrVLC-IrURC scheme when communicating over a 16QAM-modulated Rayleigh fading channel having a range of $E_b/N_0$ values.

arrangements, facilitating high-integrity operation when short interleavers are employed [27]. We note however, that the performance of all arrangements considered could be improved if more efficient designs were employed for the short interleavers, such as the $S$-random design of [28].

The SERs obtained when employing an interleaver length of $I \approx 10^6$ for each of the arrangements detailed in Section V are plotted as a function of the uncorrelated narrowband Rayleigh fading channel $E_b/N_0$ in Figure 7.

As shown in Figure 7, the SER performance of each arrangement considered exhibits a 'turbo-cliff', which is characteristic of iteratively decoded schemes. In the case of the IrVLC-IrURC-low and IrVLC-URC-low arrangements, an error floor can be seen at an SER of about $10^{-3}$. By contrast, the IrVLC-IrURC-high and IrVLC-URC-high arrangements do not exhibit an error floor for SERs above $10^{-4}$. These findings may be explained with consideration of the free distances of the VLC component codebooks that are invoked by these arrangements. More specifically, since they invoke VLC component codes having higher free distance metrics, the IrVLC-IrURC-high and IrVLC-URC-high may be expected to have higher overall concatenated free distances (and hence lower error floors) than the IrVLC-IrURC-low and IrVLC-URC-low arrangements [29].

Let us now comment on the iterative decoding complexity of the various arrangements introduced in Section V. During our simulations, in addition to recording the SER achieved after the *last* decoding iteration was performed, we also recorded the SER achieved after *each* decoding iteration, together with the cumulative number of ACS operations performed so far. In Figure 8, the average number of ACS operations per source symbol required to achieve an SER of $10^{-3}$ is plotted against $E_b/N_0$ for an average interleaver length of $I \approx 10^6$. Note that in the cases where a shorter interleaver was employed
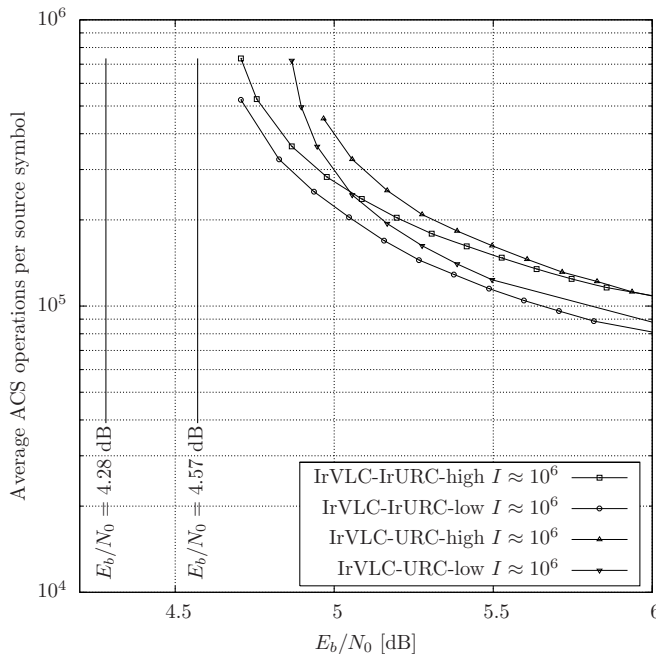
Fig. 8. Average number of ACS operations per source symbol required for the various arrangements of the IrVLC-IrURC scheme to achieve an SER of $10^{-3}$ when communicating over a 16QAM-modulated Rayleigh fading channel having a range of $E_b/N_0$ values.

and the $E_b/N_0$ value was sufficiently high to achieve an SER of $10^{-3}$, the computational complexity required was found to be roughly equal to the corresponding value provided in Figure 8 for the $I \approx 10^6$-bit interleaver.

As shown in Figure 8 for all cases considered, an SER of $10^{-3}$ may be achieved at a reduced computational complexity, as the $E_b/N_0$ value increases and the EXIT chart tunnel widens. As a result, less decoding iterations are required for reaching the particular extrinsic mutual information that is associated with an SER of $10^{-3}$. Observe in Figure 8 that the IrVLC-IrURC-high and IrVLC-IrURC-low arrangements have a lower iterative decoding complexity than the corresponding IrVLC-URC-high or IrVLC-URC-low benchmarker. This is because the benchmarkers use only the memory-3 $\mathbf{URC}^8$ code, while the IrVLC-IrURC schemes encode some bits using the lower-complexity memory-1 and memory-2 codes from the set $\{\mathbf{URC}^m\}_{m=1}^{10}$, as described in Section V. Also observe that at high $E_b/N_0$ values, the IrVLC-IrURC-low and IrVLC-URC-low arrangements have iterative decoding complexities that are approximately 25% lower than that of the corresponding IrVLC-IrURC-high or IrVLC-URC-high arrangement. This is a benefit of the modified EXIT chart matching algorithm, which facilitated the joint EXIT chart matching and the quest for a reduced computational complexity during the design of the IrVLC-IrURC-low and IrVLC-URC-low arrangements. Owing to their near-capacity performance and low iterative decoding complexity, we can identify the IrVLC-IrURC-high and IrVLC-IrURC-low arrangements as our preferred schemes.

## VII. CONCLUSIONS

In this paper we have introduced a method of performing the double EXIT chart matching of two serially concatenated

irregular codecs. This approach facilitates a higher degree of design freedom than the current state-of-the-art method of matching the EXIT chart of an irregular outer codec to that of a regular inner codec. As a result, very narrow EXIT chart tunnels can be created, facilitating operation at $E_b/N_0$ values that are closer to the DCMC capacity bound. This was demonstrated for serial concatenations of iteratively decoded IrVLCs and IrURCs, which were compared to benchmarkers, in which an IrVLC was serially concatenated with a regular URC. Our IrVLC-IrURC schemes were found to consistently achieve open EXIT chart tunnels at higher effective throughputs than the IrVLC-URC benchmarkers across a range of $E_b/N_0$ values.

Indeed, the IrVLC-IrURC schemes were found to achieve an open EXIT chart tunnel at an $E_b/N_0$ value that is just 0.04 dB from the Rayleigh fading channel's attainable capacity bound, when using an effective throughput of $\eta = 2.12$. Furthermore, our proposed schemes were found to achieve SERs of less than $10^{-3}$ for $E_b/N_0$ values in excess of 0.14 dB from the 16QAM-modulated Rayleigh fading channel's attainable capacity bound, when using an average interleaver length of approximately $10^6$ bits. These results are comparable to those of the irregular LDPC scheme proposed in [30], which achieves an open EXIT chart tunnel at 0.06 dB from the channel's $E_b/N_0$ capacity bound, in addition to facilitating operation within 0.13 dB of this bound when a $10^6$-bit block length is employed. Note however that our results may be deemed to be more radical, since [30] considers the less challenging scenario of using Binary Phase Shift Keying (BPSK) for communicating over an Additive White Gaussian Noise (AWGN) channel.

Finally, we showed that the iterative decoding complexity of our IrVLC-IrURC scheme can be reduced by about 25% upon employing a method for jointly performing EXIT chart matching and seeking a reduced iterative decoding complexity. We note however, that this complexity reduction is achieved at the cost of introducing an error floor at an SER of approximately $10^{-3}$.

## REFERENCES

[1] S. Benedetto and G. Montorsi, "Serial concatenation of block and convolutional codes," *Electron. Lett.*, vol. 32, no. 10, pp. 887–888, May 1996.

[2] ——, "Iterative decoding of serially concatenated convolutional codes," *Electron. Lett.*, vol. 32, no. 13, pp. 1186–1188, June 1996.

[3] M. Tüchler and J. Hagenauer, "EXIT charts of irregular codes," in *Proc. Conference on Information Sciences and Systems*, Princeton, NJ, USA, Mar. 2002, pp. 748–753.

[4] S. ten Brink, "Convergence of iterative decoding," *Electron. Lett.*, vol. 35, no. 10, pp. 806–808, May 1999.

[5] M. Laddomada and B. Scanavino, "Design of punctured serially concatenated convolutional codes," *IEEE Commun. Lett.*, vol. 9, no. 2, pp. 169–171, Feb. 2005.

[6] A. Ashikhmin, G. Kramer, and S. ten Brink, "Code rate and the area under extrinsic information transfer curves," in *Proc. IEEE International Symposium on Information Theory*, Lausanne, Switzerland, June 2002, p. 115.

[7] D. Divsalar, S. Dolinar, and F. Pollara, "Serial concatenated trellis coded modulation with rate-1 inner code," in *Proc. IEEE Global Telecommunications Conference*, vol. 2, San Francisco, CA, USA, Nov. 2000, pp. 777–782.

[8] J. Hagenauer, E. Offer, and L. Papke, "Iterative decoding of binary block and convolutional codes," *IEEE Trans. Inform. Theory*, vol. 42, no. 2, pp. 429–445, Mar. 1996.

[9] L. Bahl, J. Cocke, F. Jelinek, and J. Raviv, "Optimal decoding of linear codes for minimizing symbol error rate (Corresp.)," *IEEE Trans. Inform. Theory*, vol. 20, no. 2, pp. 284–287, Mar. 1974.

[10] L. Hanzo, T. H. Liew, and B. L. Yeap, *Turbo Coding, Turbo Equalisation and Space Time Coding for Transmission over Wireless Channels*. Chichester, UK: Wiley, 2002.

[11] M. Tüchler, "Design of serially concatenated systems depending on the block length," *IEEE Trans. Commun.*, vol. 52, no. 2, pp. 209–218, Feb. 2004.

[12] J. Hagenauer and R. Bauer, "The turbo principle in joint source channel decoding of variable length codes," in *Proc. IEEE Information Theory Workshop*, Cairns, Queensland, Australia, Sept. 2001, pp. 33–35.

[13] K. Lakovic and J. Villasenor, "Combining variable length codes and turbo codes," in *Proc. IEEE Vehicular Technology Conference*, vol. 4, Birmingham, AL, USA, May 2002, pp. 1719–1723.

[14] X. Jaspar and L. Vandendorpe, "New iterative decoding of variable length codes with turbo-codes," in *Proc. IEEE International Conference on Communications*, vol. 5, Paris, France, June 2004, pp. 2606–2610.

[15] K. Lakovic, T. Tian, and J. Villasenor, "Iterative decoder design for joint source-channel ldpc coding," in *Proc. EUROCON International Conference on Computer as a Tool*, vol. 1, Belgrade, Serbia and Montenegro, Nov. 2005, pp. 486–489.

[16] C. Poulliat, D. Declercq, C. Lamy-Bergot, and I. Fijalkow, "Analysis and optimization of irregular LDPC codes for joint source-channel decoding," *IEEE Commun. Lett.*, vol. 9, no. 12, pp. 1064–1066, Dec. 2005.

[17] R. Thobaben and J. Kliewer, "Low-complexity iterative joint source-channel decoding for variable-length encoded Markov sources," *IEEE Trans. Commun.*, vol. 53, no. 12, pp. 2054–2064, Dec. 2005.

[18] S. Lloyd, "Least squares quantization in PCM," *IEEE Trans. Inform. Theory*, vol. 28, no. 2, pp. 129–137, Mar. 1982.

[19] J. Max, "Quantizing for minimum distortion," *IRE Trans. Inform. Theory*, vol. 6, no. 1, pp. 7–12, Mar. 1960.

[20] R. G. Maunder, J. Wang, S. X. Ng, L.-L. Yang, and L. Hanzo, "Iteratively decoded irregular variable length coding and trellis coded modulation," in *Proc. IEEE Workshop on Signal Processing Systems*, Shanghai, China, Oct. 2007, pp. 222–227.

[21] L. Hanzo, S. X. Ng, T. Keller, and W. Webb, *Quadrature Amplitude Modulation*. Chichester, UK: Wiley, 2004.

[22] V. B. Balakirsky, "Joint source-channel coding with variable length codes," in *Proc. IEEE International Symposium on Information Theory*, Ulm, Germany, June 1997, p. 419.

[23] G. D. Forney, "Review of random tree codes," NASA Ames Research Center, Moffett Field, CA, USA, Tech. Rep. NASA CR73176, Dec. 1967.

[24] R. G. Maunder and L. Hanzo, "Genetic algorithm aided design of component codes for irregular variable length coding," accepted by *IEEE Trans. Commun.*.

[25] J. G. Proakis, *Digital Communications*. McGraw-Hill, 1983.

[26] Digital Video Broadcasting (DVB): framing structure, channel coding and modulation for digital terrestrial television, ETSI Std. EN 300 744.

[27] S. ten Brink, "Convergence behavior of iteratively decoded parallel concatenated codes," *IEEE Trans. Commun.*, vol. 49, no. 10, pp. 1727–1737, Oct. 2001.

[28] S. Dolinar and D. Divsalar, "Weight distributions for turbo codes using random and nonrandom permutations," *Telecommunications and Data Acquisition Progress Report*, vol. 122, pp. 56–65, Apr. 1995.

[29] S. B. Wicker, *Error Control Systems for Digital Communications and Storage*. Upper Saddle River, NJ: Prentice-Hall, 1994.

[30] T. J. Richardson, M. A. Shokrollahi, and R. L. Urbanke, "Design of capacity-approaching irregular low-density parity-check codes," *IEEE Trans. Inform. Theory*, vol. 47, no. 2, pp. 619–637, Feb. 2001.

**Robert G. Maunder** has studied with the School of Electronics and Computer Science, University of Southampton, UK, since October 2000. He was awarded a first class honours BEng in Electronic Engineering in July 2003, as well as a Ph.D. in Wireless Communications and a lectureship in December 2007. Rob's research interests include joint source/channel coding, iterative decoding, irregular coding and modulation techniques. He has published a number of IEEE papers in these areas.

**Lajos Hanzo,** Fellow of the Royal Academy of Engineering, received his first-class degree in electronics in 1976 and his doctorate in 1983. In 2004 he was awarded the Doctor of Sciences (DSc) degree by the University of Southampton, UK. During his career in telecommunications he has held various research and academic posts in Hungary, Germany and the UK. Since 1986 he has been with the Department of Electronics and Computer Science, University of Southampton, UK, where he holds the chair in telecommunications. He has co-authored 17 Wiley - IEEE Press books, totalling 10 000 pages on mobile radio communications, published in excess of 900 research papers, has acted as TPC Chair of numerous major IEE and IEEE conferences, presented various keynote lectures and has been awarded a number of distinctions. Currently he heads an academic research team, working on a range of research projects in the field of wireless multimedia communications sponsored by industry, the Engineering and Physical Sciences Research Council (EPSRC) UK, the European IST Programme and the Mobile Virtual Centre of Excellence (VCE), UK. He is an enthusiastic supporter of industrial and academic liaison and he offers a range of industrial courses. Lajos is also an IEEE Distinguished Lecturer and a Fellow of both the IEEE and the IEE/IET. He is an editorial board member of the Proceedings of the IEEE and a Governor of both the IEEE VT Society and ComSoc. He is the Editor-in-Chief of the IEEE Press. For further information on research in progress and associated publications, please refer to http://www-mobile.ecs.soton.ac.uk